Available online at www.sciencedirect.com
ScienceDirect
Trans. Nonferrous Met. Soc. China 32(2022) 1144−1158
Transactions of Nonferrous Metals Society of China
www.tnmsc.cn

Microstructures and mechanical properties of TC4/AZ91D bimetal prepared by solid−liquid compound casting combined with Zn/Al composite interlayer

Jian-hua ZHAO[1,2], Jing-jing SHANGGUAN[1], Cheng GU[1], Bing-yan JIN[1], Yu SHI[1]

1. College of Materials Science and Engineering, Chongqing University, Chongqing 400044, China;
2. State Key Laboratory of Mechanical Transmission, Chongqing University, Chongqing 400044, China

Received 29 April 2021; accepted 24 December 2021

Abstract: To achieve Ti/Mg bimetallic composite with high strength and metallurgical bonding interface, Al interlayer and Zn/Al composite interlayer were used to prepare TC4/AZ91D bimetal composite with metallurgical bonding interface by solid−liquid compound casting, respectively. Al interlayer was prepared on the surface of TC4 alloy by hot dipping, and Zn/Al composite interlayer was prepared by electroplating process. The results suggested that the phases across the interface were AlTi and α(Al) + $Mg_{21}(Al,Zn)_{17}$ when Zn/Al composite interlayer was used. When Al interlayer was used as interlayer, AlMgTi ternary structure and $Al_{12}Mg_{17}$ + δ-Mg eutectic structure were the main phases at the interface. The shear strength of TC4/AZ91D bimetal with Zn/Al composite interlayer was much higher than that with pure Al interlayer, and the value of the shear strength was increased from 48.5 to 67.4 MPa. Thermodynamic models based on different compositions of the interface were established to explain the microstructure evolution of the interfacial zone.

Key words: Ti/Mg bimetal composite; solid−liquid compound casting; thermodynamic analysis; microstructure; mechanical properties

1 Introduction

Ti/Mg bimetal has a great potential to be applied in automotive and aerospace fields owing to the advantages of mass reduction and fuel efficiency. The application of Ti/Mg bimetal can take advantage of not only the low density, good machinability and recyclability of magnesium alloys [1,2], but also the excellent mechanical properties, excellent corrosion resistance and high temperature resistance of titanium alloys [3−5]. Many researchers have fabricated Mg/Ti bimetal by welding technology, such as friction stir welding (FSW) [6,7], transient liquid phase (TLP) bonding [4,8], cold metal transfer (CMT) bonding [9], tungsten insert gas (TIG) welding [10], and laser welding [11−13]. However, welding process is always limited to be applied to the plate parts or the parts with simple structure, and it is not applicable for the parts with complex structure.

The process via pouring liquid metal on solid metal to connect different metals, which is called solid−liquid compound casting (SLCC), has been studied by many researchers [14−16]. The SLCC technology has the advantages of low cost, simple processing procedure and low energy consumption, which can be used for the production of the complex products. However, there is a great challenge to achieve Ti/Mg bimetal via SLCC for the low mutual dissolution [17] and positive formation enthalpy [7,18] between elements Ti and Mg. Therefore, it is necessary to use the intermediate metal to achieve the reliable metallurgical bonding between Ti and Mg. Aluminum is a good choice because it is a very

Corresponding author: Jian-hua ZHAO, Tel: +86-23-65112611, E-mail: zjhwzf@sina.com
DOI: 10.1016/S1003-6326(22)65862-X

important chemical composition in both titanium alloys and magnesium alloys. Hot-dip aluminum plating [19−23] is a method to realize metallurgical bonding between Al and Ti with complex geometries. On Al/Mg side, several methods, such as using Zn interlayer [14], have been adopted to avoid the direct formation of $Al_{12}Mg_{17}$ intermetallic compound for its high hardness and brittleness at the interface.

In this work, a simple and applicable method was developed to prepare TC4/AZ91D bimetal. The reliable metallurgical bonding of TC4/AZ91D bimetal composite was realized by using Zn/Al composite interlayer. The evolution mechanism of the interface was established by combining the interfacial thermodynamic model and the composition of the interface.

2 Experimental

2.1 Material preparation

TC4 (Ti−6wt.%Al−4wt.%V) titanium alloy with the diameter of *d*5 mm was chosen as the solid insert. AZ91D (Mg−9wt.%Al−1wt.%Zn) magnesium alloy ingots were selected as the melt material. The chemical compositions of TC4 and AZ91D were summarized in Table 1. Pure aluminum ingots were used as the coating material, which were coated on the surface of TC4 rods by hot dipping technology. RJ-2 flux was chosen as covering flux of magnesium alloy to prevent melting from oxidation.

2.2 Preparation of Zn/Al composite interlayer

Before coating process, TC4 rods were cut into 40 mm in length by an electrical discharge machine and treated by hydrofluoric acid (HF) and nitric acid (HNO_3) to remove the oxides. To prevent the surface of the TC4 rods from being oxidized before coating, TC4 rods were placed in a saturated solution of K_2ZrF_6 at 80 °C for 5 min. The treated TC4 rods were then dipped into pure Al melt at 700 °C for 10 min. At last, Zn layer was prepared on the surface of Al-coated TC4 rods by electroplating zinc technology at room temperature. The mechanisms of alumina dissolution and zinc deposition are summarized as follows:

$$Al_2O_3+2OH^-\rightarrow 2AlO^{2-}+H_2O \quad (1)$$

$$Al+3[Zn(OH)]^{2-}\rightarrow 3Zn+2[Al(OH)_4]^-+4OH^- \quad (2)$$

The preparation parameters are shown in Table 2. TC4 insert without interlayer was chosen as a comparison group, which was treated by the above method without coating. Figures 1 and 2 show the SEM images and EDS results of TC4 rods with Al and Zn/Al composite coatings, respectively. Figure 1(a) shows the BSE image of Al-coated TC4, and the corresponding EDS line scan is shown in Fig. 2. Figure 1(b) shows the surface morphology of Al-coated TC4 rod. As can be seen, there are two layers formed on the surface of TC4 rod after hot dipping Al process. Based on the EDS line scan results and the research of NASSIK et al [24], it can be deduced that $TiAl_3$ is the only product during hot

Table 1 Chemical compositions of materials (wt.%)

Material	Al	Zn	Mn	Si	Fe	Ni	Cu	V	Ti	Mg
TC4	5.5−6.8	−	−	−	≤0.3	−	−	3.5−4.5	Bal	−
AZ91D	8.5−9.0	0.45−0.5	0.17−0.4	≤0.05	≤0.004	≤0.01	≤0.02	−	−	Bal

Table 2 Preparation parameters of Al−Zn composite interlayer

Process	Parameter
Degreasing	25 g/L Na_2CO_3 + 30 g/L Na_3PO_4, 70 °C, 5 min
Alkali washing	100 g/L NaOH, room temperature, 20 s
Acid pickling	50% HNO_3 + 48% HF + 2% H_2O, room temperature, 10 s
First zinc treatment	50 g/L NaOH + 5 g/L ZnO + 50 g/L $KNaC_4H_4O_6$ + 1 g/L $NaNO_3$, room temperature, 40 s
Zinc retreatment	HNO_3 (60%), room temperature, 30 s
Second zinc treatment	120 g/L NaOH + 20 g/L ZnO + 50 g/L $KNaC_4H_4O_6$ + 1 g/L $NaNO_3$ + 1 g/L $FeCl_3$, room temperature, 20 s
Electroplating zinc	12 g/L ZnO + 130 g/L NaOH + 60 mL/L additive agent ZN-1A, room temperature, 20 min

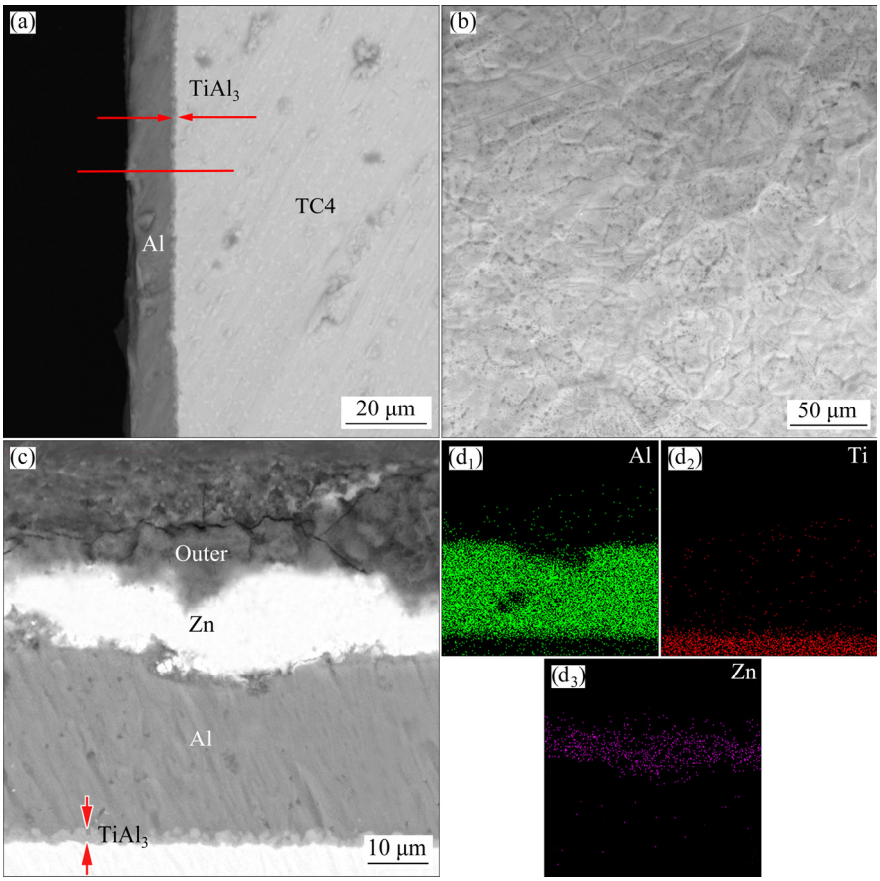

Fig. 1 Microstructures of TC4 rods with different layers: (a) Al-coated TC4; (b) Surface of Al-coated TC4; (c) Zn/Al-coated TC4; (d_1−d_3) Element distribution of (c)

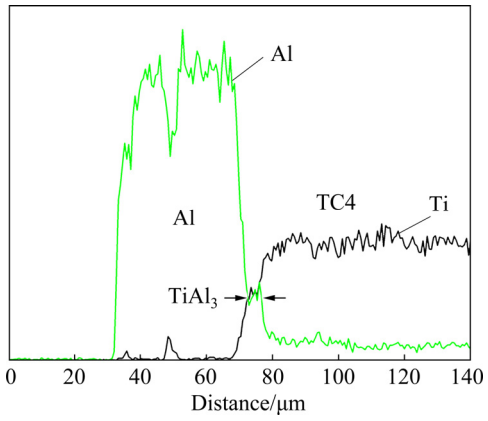

Fig. 2 EDS line scan spectra according to red line in Fig. 1(a)

dipping Al process of Ti. A layer of pure Al coating is attached to the surface of TC4 rod when TC4 rod is extracted from Al melt, which has a thickness of 20 μm. Figure 1(c) shows the BSE image of Zn/Al-coated TC4 rod, and the EDS mapping scan results are presented in Figs. 1(d_1−d_3). It is revealed that there are clear boundaries between Zn and Al coatings, indicating that there is no intermetallic layer formed between Zn coating and Al coating.

2.3 Compound casting

Solid−liquid compound casting was conducted between Zn/Al-coated TC4 substrate and AZ91D alloy. Figure 3 illustrates the schematic diagrams of the compound casting, and the shape and dimensions of the casting mold. The mold was preheated at 250 °C for 2 h and Zn/Al-coated TC4 rod was placed in the mold before casting. And then, AZ91D melt was poured into the mold with a steady speed as the temperature reached the designed temperature (720 and 750 °C). TC4/AZ91D bimetal could be taken out from the mold after the casting solidified completely. Figure 4 shows the temperature−time curves recorded by paperless recorder when the casting temperature is 720 and 750 °C, respectively.

2.4 Characterization

The interface microstructure and the fracture surfaces of the samples were observed by a TESCAN VEGA 3LMH scanning microscope (SEM). The microstructures of the interface were characterized by JEM−2100F microscope operated

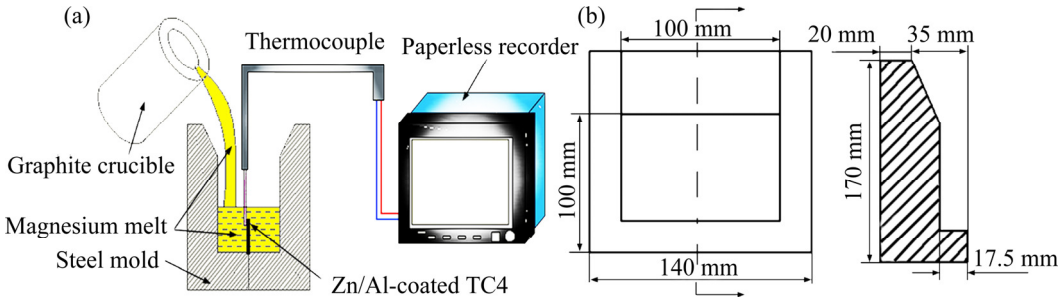

Fig. 3 Schematic diagrams of casting process (a) and CAD drawing of one casting mold half (b)

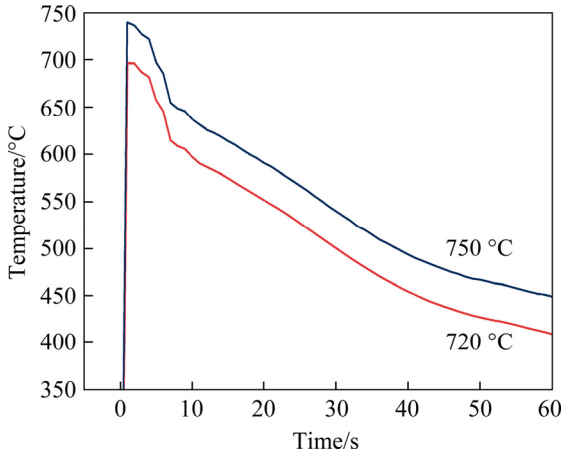

Fig. 4 Temperature−time curves recorded by paperless recorder at casting temperatures of 720 and 750 °C

at 200 kV in transmission electron microscope (TEM) using scanning transmission electron microscope (STEM) and high resolution (HRTEM) modes, respectively. The distribution and content of elements were analyzed by the energy dispersive X-ray spectrometer (EDS) detector. The Vickers microhardness tests were conducted at the interface of samples by using an MH−5L microhardness tester under the load of 10 g and the time was 15 s. An adequate spacing of indentations was ensured to avoid the interference between adjacent ones.

The adhesive strength between TC4 titanium alloy and AZ91D magnesium alloy was measured by shear test. The schematic sketch of the shear test is illustrated in Fig. 5. The shear strength of the interface (δ_τ) could be calculated based on the equation as follows:

$$\delta_\tau = \frac{F_{\max}}{\pi D h} \tag{3}$$

where $F_{\max}$ is the maximum load, h is the height of sample, and D is the diameter of the specimen.

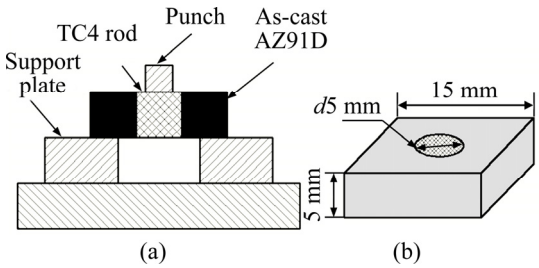

Fig. 5 Schematic diagram of shear test (a) and size of shear test sample (b)

2.5 Thermodynamic analysis

In order to investigate the effects of Zn/Al coating on the evolution of interfacial zone, Gibbs free energy, formation enthalpy, and chemical potential of Al−Ti−Zn and Al−Mg−Zn ternary systems were calculated in this study. The chemical potential can be expressed by the following equation:

$$\mu_i = \frac{\partial G}{\partial x_i} \tag{4}$$

where μ_i is the chemical potential of element i, G is the Gibbs free energy of the system, and x_i is the molar fraction of i.

The real solution Gibbs free energy G is the summation of the ideal solution molar Gibbs free energy G^{I} and the excessive molar Gibbs free energy G^{E}. G^{I} and G^{E} could be expressed by the following equations:

$$G^{\mathrm{I}} = x_i G_i^* + x_j G_j^* + x_k G_k^* + RT(x_i \ln x_i + x_j \ln x_j + x_k \ln x_k) \tag{5}$$

$$G^{\mathrm{E}} = \frac{x_j}{1-x_i} G_{i,j}^{\mathrm{E}}(x_i, 1-x_i) + \frac{x_k}{1-x_i} G_{i,k}^{\mathrm{E}}(x_i, 1-x_i) + (x_i + x_k)^2 G_{j,k}^{\mathrm{E}}\left(\frac{x_j}{x_j + x_k}, \frac{x_k}{x_j + x_k}\right) \tag{6}$$

where G_i^*, G_j^* and G_k^* are the molar Gibbs free energies of pure components i, j and k, respectively. x is the molar fraction of the corresponding component, R is the molar gas constant, and T is the system temperature. $G_{i,j}^E$ is the excessive molar Gibbs free energies of the binary system which can be calculated by

$$\Delta G_{i,j}^{\mathrm{E}} = \Delta H_{i,j} - T\Delta S_m^{\mathrm{E}} \tag{7}$$

where $\Delta H_{i,j}$ is the formation enthalpy change which can be expressed as

$$\begin{aligned}\Delta H_{i,j} = f_{i,j}\{x_i[1+\mu_i x_j(\varphi_i-\varphi_j)x_j]\cdot \\ [1+\mu_j x_i(\varphi_j-\varphi_i)]\}/\{x_i V_i^{2/3}[1+u_i x_j(\varphi_i-\varphi_j)]+ \\ x_j V_j^{2/3}[1+u_j x_i(\varphi_j-\varphi_i)]\}\end{aligned} \tag{8}$$

$$f_{i,j} = \frac{2pV_i^{2/3}V_j^{2/3}[q/p(\Delta n_{\mathrm{ws}}^{1/3})^2-(\Delta\varphi)^2-\alpha(r/p)]}{(\Delta n_{\mathrm{ws}}^{1/3})_i^{-1}+(\Delta n_{\mathrm{ws}}^{1/3})_j^{-1}} \tag{9}$$

The formation enthalpy of ternary system can be calculated by Miedema model [25]:

$$\begin{aligned}\Delta H_{i,j,k} = &\frac{x_j}{1-x_i}\Delta H_{i,j}\left(x_i, 1-x_i\right)+ \\ &\frac{x_k}{1-x_i}\Delta H_{i,k}\left(x_i, 1-x_i\right)+ \\ &\left(x_j+x_k\right)^2\Delta H_{j,k}\left(\frac{x_j}{x_j+x_k}, \frac{x_k}{x_j+x_k}\right)\end{aligned} \tag{10}$$

where φ, V and n_{ws} are the parameters which represent electronegativity, molar volume and electron density parameter, respectively. q, r, u, α and p are experimental constants. The parameters adopted in this study are listed in Table 3, which are determined by Miedema model [25]. $\Delta S_{\mathrm{m}}^{\mathrm{E}}$ is the excessive entropy change and can be expressed as follows:

$$\Delta S_{\mathrm{m}}^{\mathrm{E}} = \Delta H_{i,j}(1/T_{\mathrm{m},i}+1/T_{\mathrm{m},j})/14 \tag{11}$$

where T_{m} is the melting point.

Table 3 Parameters adopted of Mg, Ti, Al, and Zn elements

Element	T_{m}/K	n_{ws}/d.u.	φ/V	u	V/cm^3	r/p
Mg	922	1.60	3.45	0.1	14.00	0.4
Ti	1933	3.51	3.8	0.04	10.58	1.0
Al	933	2.70	4.2	0.07	10.58	1.9
Zn	693	2.30	4.1	0.1	9.23	1.4

The above formulas were used to calculate the Gibbs free energy, formation enthalpy and chemical potential of Al−Ti−Zn and Al−Mg−Zn ternary systems, which could be helpful to explain the evolution of the interfacial zone.

3 Results and discussion

3.1 Effects of pure Al coating on microstructure of TC4/AZ91D bimetal

In order to highlight the necessity of this study, TC4/AZ91D bimetal without interlayer was used as a contrast. The thermodynamic calculation of Ti/Mg binary system is presented in Fig. 6. As can be seen in Fig. 6, the Gibbs free energy change of Ti/Mg pure element ($\Delta G_{\mathrm{Ti/Mg}}$) and Gibbs free energy change of the alloying ($\Delta G_{\mathrm{alloying}}$) between the immiscible metals at the interface are both positive, which indicates that Mg and Ti elements could not react spontaneously. The cross-section microstructure of TC4/AZ91D bimetallic material without interlayer was observed by SEM as shown in Fig. 7. As a result, there is no metallurgical bonding between TC4 and AZ91D substrates.

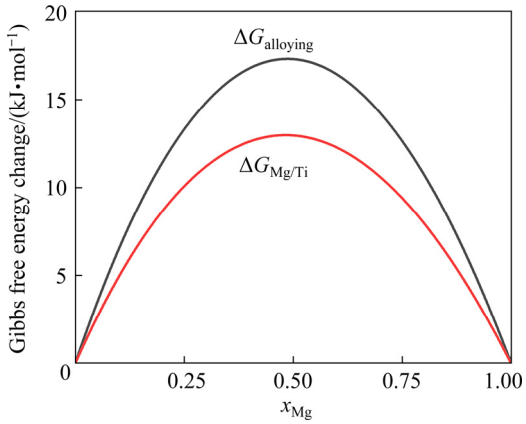

Fig. 6 Gibbs free energy change of Mg−Ti binary system

Figure 8 shows the SEM images of Al-coated TC4/AZ91D bimetal cast at 720 °C and the corresponding EDS line result. As can be seen, a metallurgical bonding zone about 25 μm in width is formed between TC4 and AZ91D substrates. Two different reaction zones can be divided based on the EDS line scan spectra in Fig. 8(c). One is the metallurgical reaction that occurs between Al and Ti, and the other is the reaction between Al and Mg. The high magnification image of Area A is shown in Fig. 8(b), and the EDS point results are summarized in Table 4. It can be concluded that

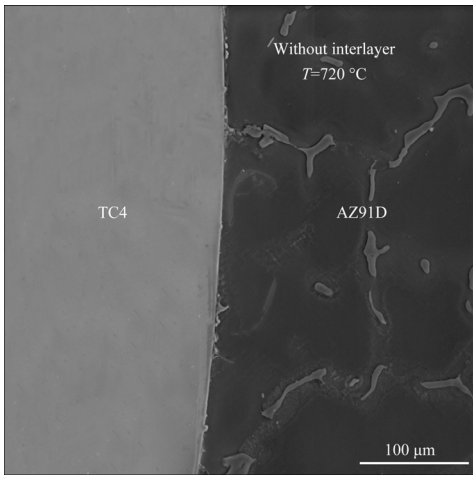

Fig. 7 SEM image of cross-section of TC4/AZ91D bimetallic materials without interlayer

the interfacial zone of Al-coated TC4/AZ91D bimetal with pure Al coating mainly consists of $Al_{12}Mg_{17}$ + δ-Mg eutectic structure. Because the amount of Mg atoms varies in the interfacial zone, $Al_{12}Mg_{17}$ phase presents two different morphologies. The formation of $Al_{12}Mg_{17}$+δ-Mg eutectic structure is based on the eutectic transformation at 437 °C:

$$L \rightarrow \delta\text{-Mg}+Al_{12}Mg_{17} \quad (12)$$

The outside of the interfacial zone has the high content of Mg, and $Al_{12}Mg_{17}$ phase grows towards the depth of Mg melt and shows an interdendritic structure. In the inner region of the interfacial zone, since Mg melt solidifies quickly, Mg atoms are all surrounded by Al atoms, and the honeycomb structure of $Al_{12}Mg_{17}$+δ-Mg eutectic structure appears to be non-directional.

It is worth noting that about 12.34 at.% Mg element appears at Point 1, and the morphology of this layer has a significant change compared with that before casting. In order to investigate the difference of Layer I before and after casting, SAED pattern of $TiAl_3$ layer before casting is presented in Fig. 8(d). The HRTEM image of this position and its FFT pattern (insert) is presented in Fig. 8(e). As can be seen in Fig. 8(d), $TiAl_3$ phase is confirmed as a single crystal and tetragonal structure [26] (a=0.386 nm, c=0.864 nm). However, the FFT pattern of Point 1 exhibits polycrystalline structure. According to the calculations of FANG and FAN [27], and HU et al [28], the above structure is confirmed to be the structure of DO_{22}-$TiAl_3$. Therefore, it can be concluded that some Mg atoms enter $TiAl_3$ interlayer and replace Al atoms, forming AlMgTi ternary structure.

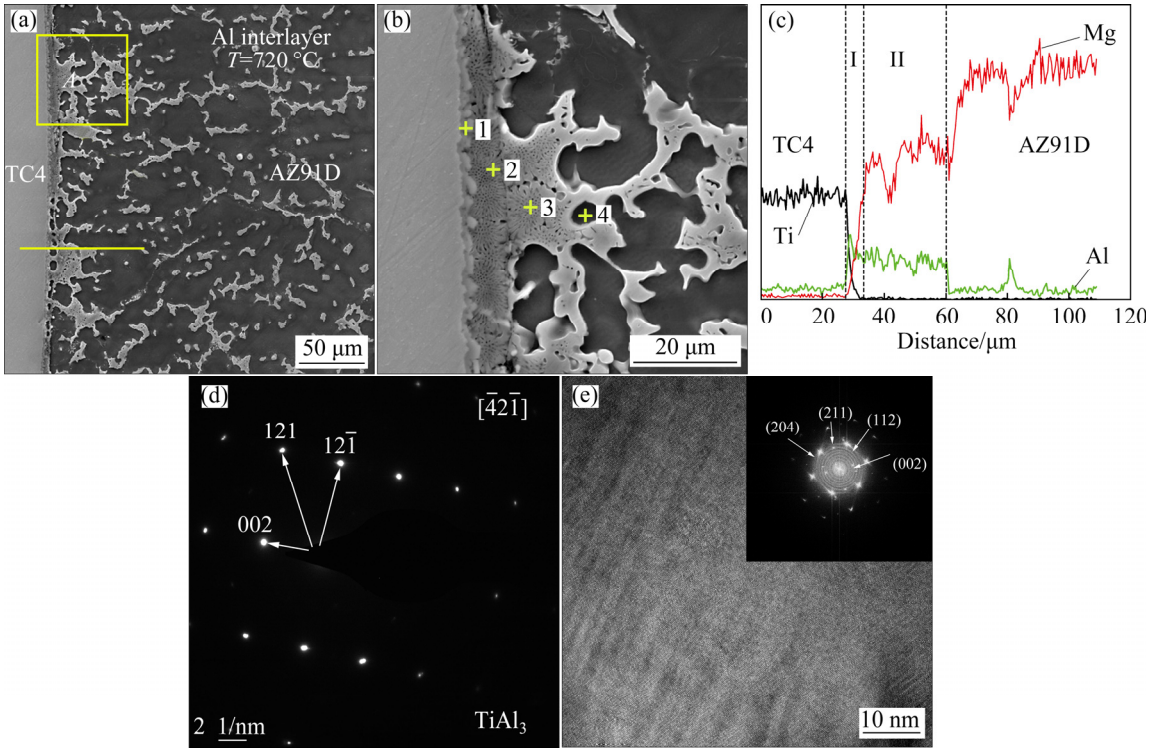

Fig. 8 SEM images and corresponding TEM analysis of cross-section of Al-coated TC4/AZ91D bimetal: (a) General structure; (b) Area A in (a); (c) EDS line scan according to yellow line in (a); (d) SAED pattern of $TiAl_3$ layer before casting; (e) HRTEM image at Point 1 and corresponding FFT pattern (insert)

Table 4 EDS analysis results of Points 1−4 in Fig. 8

Point	Element (at. %)			Possible phase
	Ti	Mg	Al	
1	27.59	12.34	60.07	AlMgTi
2	−	63.03	36.97	$Al_{12}Mg_{17}$
3	−	63.65	36.35	$Al_{12}Mg_{17}$
4	−	89.39	10.61	δ-Mg

The above analysis proves that the metallurgical bonding zone can be formed between Al-coated TC4 and AZ91D substrates. The main composition of the interfacial zone is δ-Mg+$Al_{12}Mg_{17}$ eutectic structure due to the metallurgical reaction, which is similar to the interfacial zone of Al/Mg bimetallic materials. However, $Al_{12}Mg_{17}$ phase is the intermetallic compound with a high hardness and brittleness [14]. It is necessary to take measures to prevent the direct reactions between aluminum and magnesium.

3.2 Effects of Zn/Al composite interlayer on microstructure of TC4/AZ91D bimetal

The microstructures of cross-sections of Zn/Al-coated TC4/AZ91D bimetallic materials were observed by SEM, as shown in Fig. 9. As can be seen in Fig. 9(a), with the application of Zn/Al composite interlayer, the metallurgical reactions take place between Al, Mg and Zn elements, and Al atoms no longer react with Mg atoms directly. According to EDS line scan results shown in Fig. 10(a), the interfacial zone can be divided into two different layers. The layer next to TC4 substrate consists of Al and Ti elements, and the layer on AZ91D side mainly consists of Al, Mg and Zn elements. High magnification image of Area *A* marked in Fig. 9(a) is shown in Fig. 9(b). A large number of white granular phases appear in the gray blocky phase. TEM technology was used to investigate the interface composition of Zn/Al-coated TC4/AZ91D bimetal materials, as shown in Fig. 11.

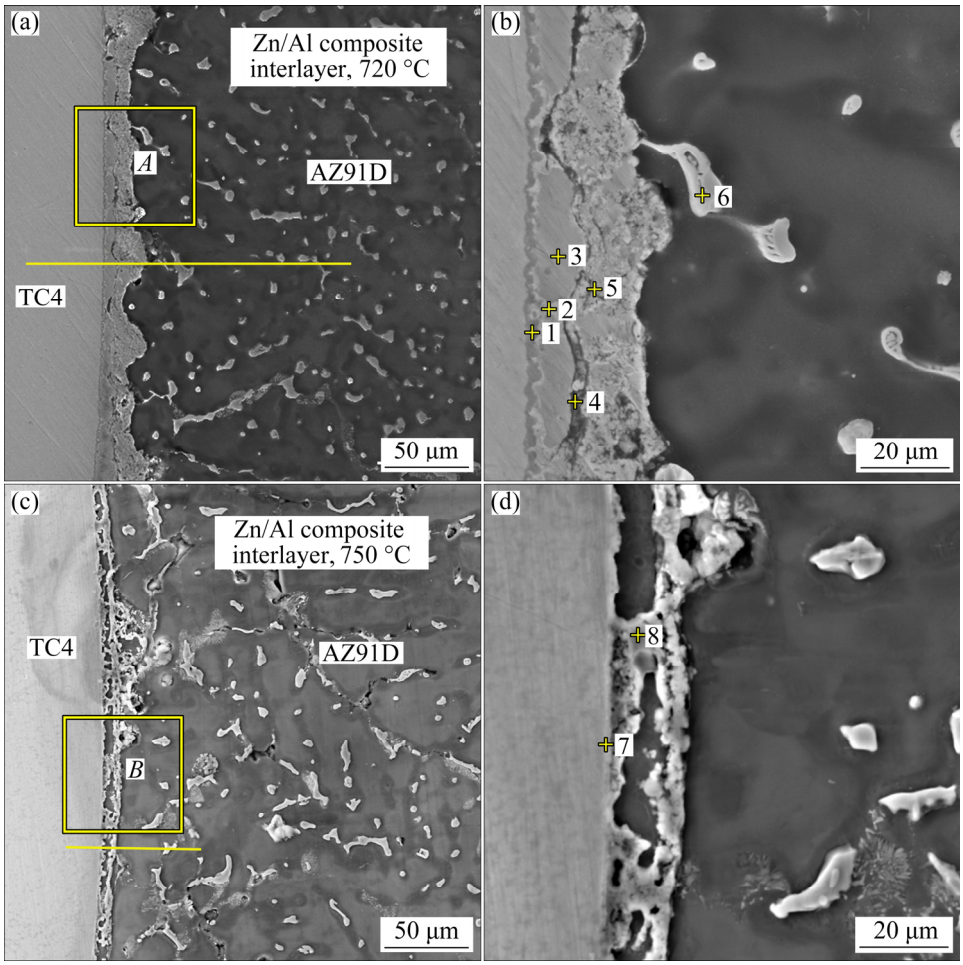

Fig. 9 SEM images of TC4/AZ91D bimetal with Zn/Al composite interlayer: (a) General view cast at 720 °C; (b) Area *A* in (a); (c) General view cast at 750 °C; (d) Area *B* in (c)

Figure 11(a) displays the microstructure of Zn/Al-coated TC4/AZ91D bimetal material using TEM technology. As can be seen in Fig. 11(a), the connections between different layers are relatively tight. The EDS mapping results present the elements distribution of different layers, which suggests that the distribution of Mg and Zn is similar, as shown in Figs. 11(b_1−b_4). Al element is significantly distributed in both AlTi and AlMgZn layers, indicating that the use of Zn interlayer prevents Mg from reacting directly with Al. In order to study the composition of AlMgZn layer, the magnification of Area *A* in Fig. 11(a) is shown in Fig. 11(c), where a lot of rod-like phases containing

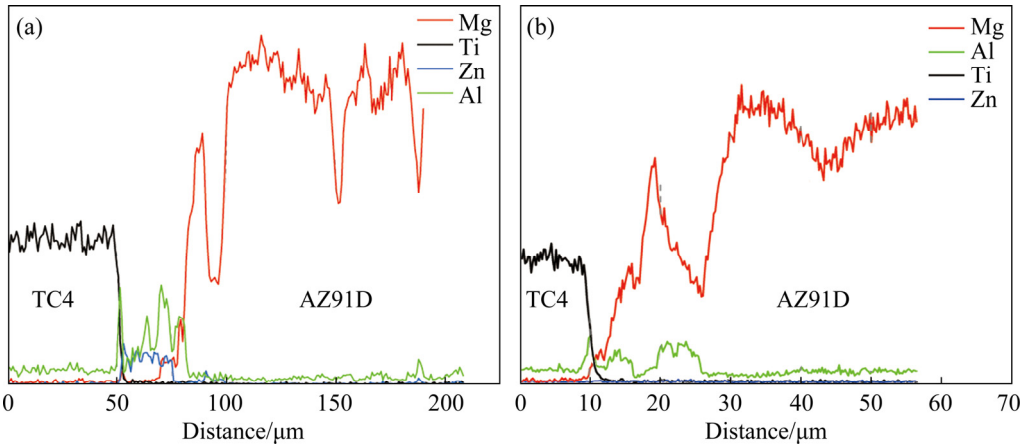

Fig. 10 EDS line scan spectra according to yellow lines in Fig. 9: (a) Fig. 9(a); (b) Fig. 9(c)

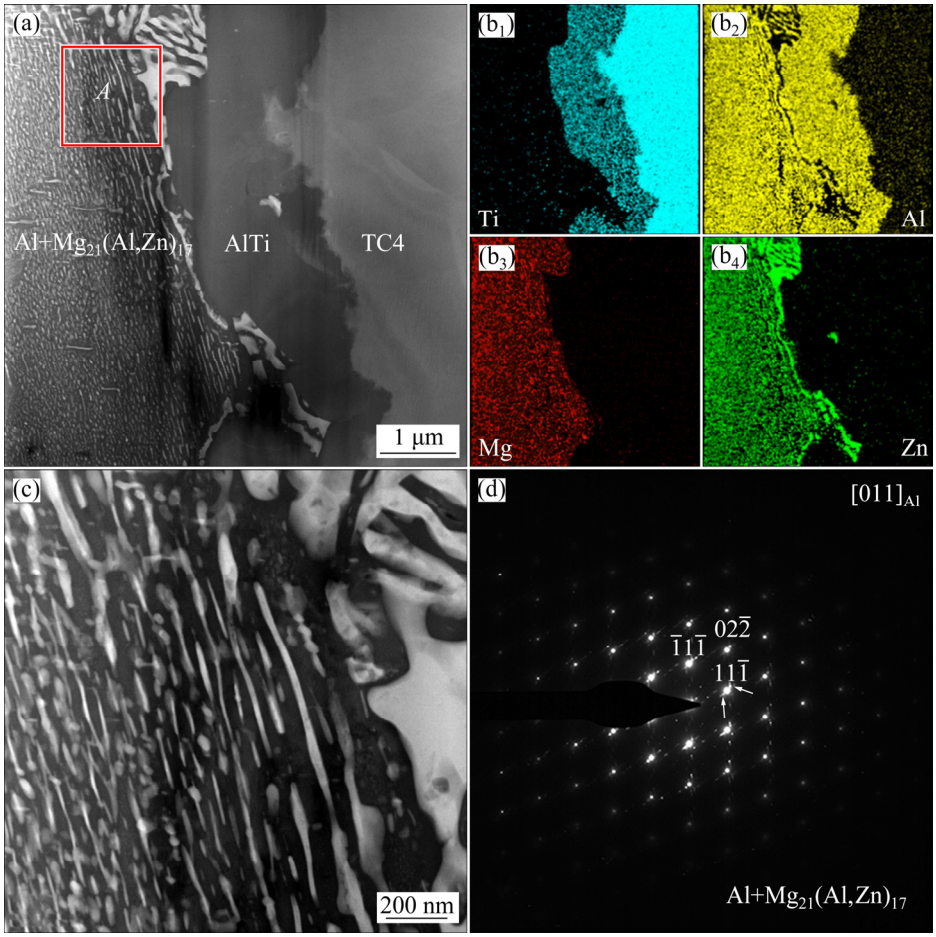

Fig. 11 TEM images of cross-sections of Zn/Al-coated TC4/AZ91D bimetal: (a) Dark-field image of different interlayers; (b_1−b_4) EDS mapping results of elements distribution; (c) High magnification of Area *A* in (a); (d) SAED pattern of Al+$Mg_{21}(Al,Zn)_{17}$ taken along $[011]_{Al}$ orientation

Al, Mg and Zn elements can be found. The SAED pattern taken along $[011]_{Al}$ is shown in Fig. 11(d). Based on the EDS point results (Table 5) and the SAED pattern, it can be deduced that the matrix structure is α(Al), and $Mg_{21}(Al,Zn)_{17}$ phases appear on Al matrix as precipitated phases. It should be noted that diffraction spots of $Mg_{21}(Al,Zn)_{17}$ phase indicated by the arrows in Fig. 11 are elongated, while the spots of Al are undistorted, suggesting that $Mg_{21}(Al,Zn)_{17}$ phases have plastic deformation with respect to Al matrix, which is helpful to change the brittle interface between Al and Mg. Figure 11(c) also suggests that no Mg spots appear on Al + $Mg_{21}(Al,Zn)_{17}$ side, indicating that the composition of Point 8 in Fig. 9(d) is δ-Mg due to the limited Zn and Al element in the interlayer. The part of Mg, which cannot react with Al and Zn, will precipitate again after entering the interlayer in large quantities.

Table 5 EDS results of Points 1−8 in Fig. 9

Point No.	Element content/at.%			
	Ti	Mg	Al	Zn
1	50.30	−	48.56	1.14
2	−	59.67	15.90	24.43
3	−	−	79.37	20.63
4	−	89.13	5.65	5.22
5	−	14.93	47.50	37.57
6	−	69.12	18.45	12.43
7	31.80	18.79	49.41	−
8	−	68.45	30.28	1.23

As the pouring temperature increases to 750 °C, as shown in Fig. 9(c), many dispersed rod-like phases and defects appear in the interfacial zone. The high magnification image of Area *B* marked in Fig. 9(c) is shown in Fig. 9(d). It can be found in Fig. 9(d) that, Al and Zn interlayers melt immediately, and the interfacial zone of $Al_{12}Mg_{17}$+ δ-Mg eutectic structure is formed according to the EDS point results.

The layer next to TC4 substrate mainly consists of 50.30 at.% Ti and 48.56 at.% Al. TEM technology was also used to investigate the composition of this layer. Figures 12(a−c) show the STEM image and the corresponding SAED patterns of the interface between TC4 substrate and AlTi interlayer, respectively. As can be seen in Figs. 12(b) and (c), both AlTi interlayer and TC4 substrate are single-crystal structure. However, the SAED pattern in Fig. 12(b) shows that neither visible secondary particles nor extra spots (only Ti spots) can be observed, suggesting the full dissolution of Al phase. However, some Al diffraction spots (as indicated by arrows) appear at Fig. 12(c), suggesting that the lattice distortion occurs in TiAl interlayer, which is caused by diffusion process. In order to find the dominant element in the diffusion process between TC4 substrate and AlTi interlayer, HRTEM image of the interface is displayed in Fig. 12(d). It is evident that there is a transition zone between TC4 substrate and AlTi interlayer. Figure 12(e) shows the magnified image and its inverse Fourier transformation (IFFT) pattern of Fig. 12(d), which suggests that the transition zone is Ti atoms. The results indicate that Ti atoms move from TC4 substrate to AlTi interlayer.

3.3 Thermodynamic calculation

According to the elements distribution of the interfacial zone before casting, two different regions under different thermodynamic conditions can be distinguished. They are, Al−Mg−Zn and Ti−Al−Zn ternary systems. In this work, the thermodynamic models based on TOOP [29] and MIEDEMA [25] models have been calculated and analyzed. Figure 13 shows the Gibbs free energy change, formation enthalpy change and chemical potential gradient of different systems, which is helpful to explain the formation mechanism of the interfacial zone.

Based on the EDS results, the Mg content is over 59 at.% in areas where AlMgZn ternary phases are concentrated. As a result, it is not necessary to discuss the condition of Mg content less than 59 at.%. In these regions, the value of ΔG_m increases with the increase of Al content, which means that the thicker the Al coating contacts with AZ91D melt, the more difficult the formation of AlMgZn ternary phases is. There are a large number of Mg atoms entering the interfacial zone with AZ91D melt during the casting process. A part of these atoms which cannot participate in the reaction have to precipitate as δ-Mg during the solidification process, as shown in Point 4 in Fig. 9(b). Compared with Al−Mg−Zn ternary system, the formation of $TiAl_3$ phase prevents Ti atoms from reacting directly with Al atoms. As can

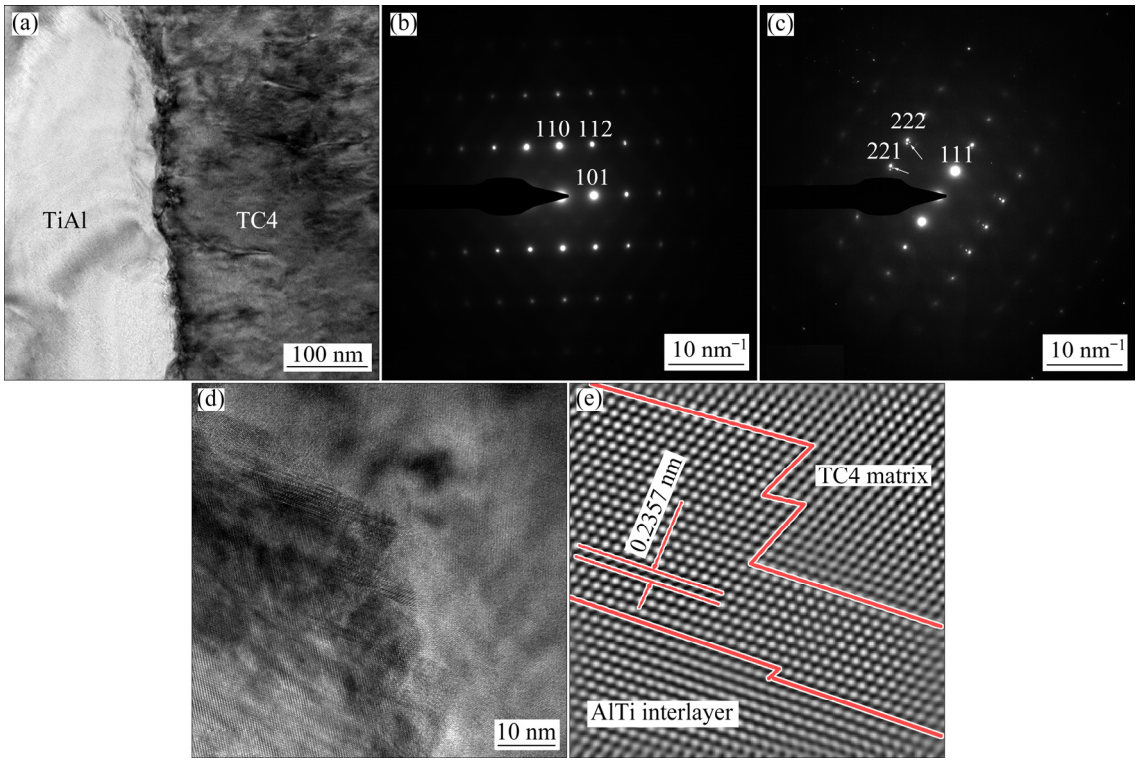

Fig. 12 STEM micrograph of interface between TC4 substrate and AlTi interlayer (a), SAED pattern of TC4 substrate (b), SAED pattern of TiAl interlayer (c), HRTEM image of interface (d), and magnified image and IFFT pattern (e) of (d)

be seen in Fig. 13(b), the value of ΔG_m at the line of $TiAl_3$ does not change much with the change of Zn content.

Figure 13(c) shows the formation enthalpy change of Al−Mg−Zn ternary system. Mg atoms in the melt are more likely to react with Zn atoms in the coating. As Al coating melts, the value of ΔH increases with the increase of Al content in the system. Therefore, the application of Zn coating will reduce the thermodynamic conditions for the formation of $Al_{12}Mg_{17}$ intermetallic compound. Thermodynamic analysis results have been verified by the above experiments. $Mg_{21}(Al,Zn)_{17}$ + α(Al)(Zn) structure takes place of $Al_{12}Mg_{17}$ + δ-Mg eutectic structure in the interfacial zone, as shown in Fig. 9.

The above analysis shows that the diffusion tendency of Al atoms in the fusion zone determines the evolution and composition of the interfacial zone. It is necessary to discuss the chemical potential of Al element in Al−Mg−Zn and Al−Ti−Zn ternary systems. The chemical potential gradients ($\Delta\mu_{Al}$) of Al in Al−Mg−Zn and Al−Ti−Zn systems are shown in Figs. 13(e) and (f), respectively. In Al−Mg−Zn system, Al atoms tend to diffuse to Zn atoms, suggesting that it is easy for the formation of α(Al)(Zn). AlMgZn ternary phases start to form as Zn content increases. As can be seen in Fig. 13(f), the chemical potential gradient of Al to $TiAl_3$ is much lower than that of Al to Zn. Ti atoms on TC4 substrate can only react with $TiAl_3$ intermetallic compound and form AlTi intermetallic compound on the TC4 side.

3.4 Mechanical properties of TC4/AZ91D bimetal

The Vickers microhardness profiles across the interfacial zone of TC4/AZ91D bimetal cast at 720 °C are displayed in Fig. 14(a). Since the sample cast at 750 °C has no obvious metallurgical bonding interface, it is not necessary to study the microhardness distribution of these samples. As can be seen in Fig. 14(a), the microhardness of TC4 and AZ91D substrates is HV 340 and HV 45, respectively. The microhardness of the interfacial zone next to the TC4 substrate is higher than that of TC4 substrate, which is due to the formation of TiAl and MgAlTi intermetallic compounds with

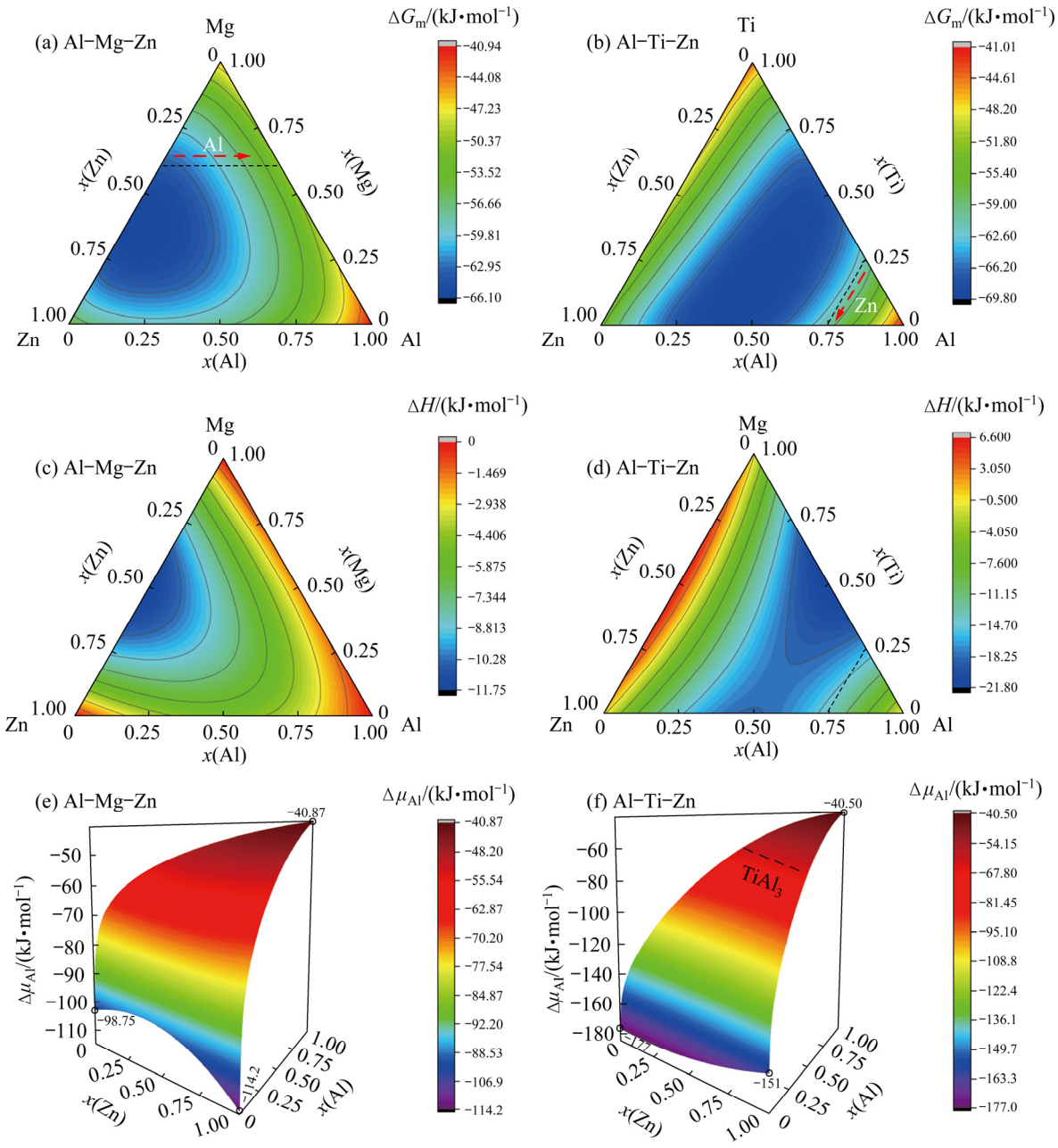

Fig. 13 Thermodynamic calculation of Al−Mg−Zn and Al−Ti−Zn ternary systems: (a, b) Gibbs free energy change; (c, d) Formation enthalpy change; (e, f) Chemical potential gradient

higher hardness. For the sample of Al-coated TC4/AZ91D bimetal, Layer II has higher microhardness than AZ91D substrate due to the formation of $Al_{12}Mg_{17}$ intermetallic compound and the value is HV 182. For the sample of Zn/Al-coated TC4/AZ91D bimetal, the microhardness of α(Al)(Zn) + $Mg_{21}(Al,Zn)_{17}$ structure is relatively low due to the existence of α(Al)(Zn) solid solution. The microhardness is HV 71 and HV 117 on the TC4 side and AZ91D side, respectively.

The mechanical properties were investigated to estimate the adhesive strength between TC4 and AZ91D. Figure 14(b) shows the shear strength of TC4/AZ91D bimetals under different conditions. As can be seen in Fig. 14(b), the average shear strength of TC4/AZ91D bimetal without interlayer is 13.5 MPa. With the use of pure Al interlayer, the shear strength is 48.5 MPa due to the metallurgical reaction between TC4 and AZ91D, but the shear strength decreases with the increase of casting temperature. When Zn/Al composite coating is used as the interlayer, the shear strength gets further improvement, and the shear strength is 67.4 MPa. It proves that the α(Al)(Zn) + $Mg_{21}(Al,Zn)_{17}$ structure

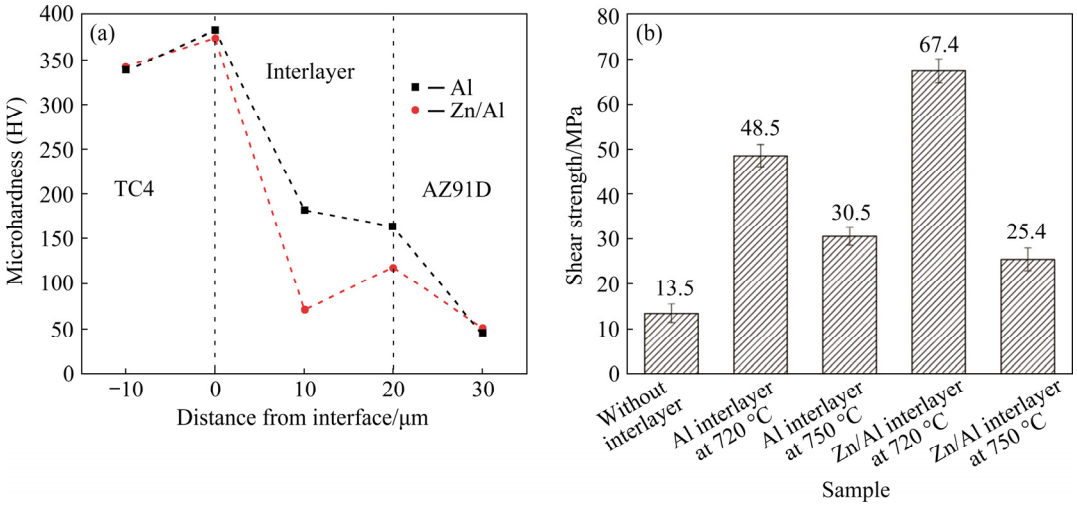

Fig. 14 Mechanical properties of TC4/AZ91D bimetal with different interlayers: (a) Microhardness distribution; (b) Shear strength

has higher bonding strength than that of $Al_{12}Mg_{17}$+ δ-Mg eutectic structure. However, the shear strength drops to 25.4 MPa when the casting temperature is 750 °C.

In order to analyze the fracture behavior of TC4/AZ91D bimetal, the fractured location and surface were observed by SEM. Figure 15 shows the fracture morphology of the Al-coated TC4/AZ91D and Zn/Al-coated TC4/AZ91D bimetals cast at 720 °C. Both the samples have obvious metallurgical bonding zone. As can be seen in Fig. 15(a), the fracture occurs almost on the surface of TC4 substrate, which suggests that the fracture occurs at $Al_{12}Mg_{17}$ + δ-Mg eutectic structure. Figure 15(b) shows the typical fracture surface of the TC4/AZ91D bimetal with Al interlayer, and the brittle fracture surface is relatively flat. With the use of Zn/Al composite interlayer, the distance from TC4 substrate to fracture is about 10 μm (Fig. 15(c)), which indicates that the rupture occurs on the junction of Zn-rich and Al-rich sides, where δ-Mg is precipitated. The corresponding typical fracture surface is shown in Fig. 15(d), and the step-like brittle fracture shows a directional height difference.

3.5 Mechanism of TC4/AZ91D bimetal with Zn/Al composite interlayer

Figure 16 illustrates the interface model in the TC4/AZ91D bimetal. The model was built based on the overall interface structure. It reveals the characteristics and details of the interface microstructure, which is helpful to explain the whole process of the growth of interfacial zone. As presented in Fig. 16(a), Mg−Ti and Al−Zn cannot react spontaneously due to the positive formation enthalpy change. Based on the research of KEŞLIOĞLU and MARAŞLI [30], the reaction between Al and Zn elements is due to solid solution diffusion. By contrast, the spontaneous reaction of Mg−Zn and Al−Ti binary systems is easier. The microstructure evolution can be divided into four stages: (1) Before casting, the whole system consists of TC4 substrate, $TiAl_3$ intermetallic compound layer, Al coating, and Zn coating, as shown in Fig. 16(b). (2) During the casting process, Mg and Zn atoms begin to involve into the reaction layer, and Al coating is gradually melted. Meanwhile, Ti atoms move towards the $TiAl_3$ intermetallic compound layer, as shown in Fig. 16(c). (3) The transfer of heat is from AZ91D melt to TC4 substrate, resulting in an uneven distribution of atoms in each interfacial layer. The distribution of different atoms is shown in Fig. 16(d). (4) During the solidification process, α(Al)(Zn)+Mg_{21}(Al,Zn)$_{17}$ structure is formed in the interfacial zone due to the lowest formation enthalpy. The value of ΔG_m increases as the distance from AZ91D increases, which leads to the difficulty to form Mg_{21}(Al,Zn)$_{17}$ ternary phases. The excessive Mg atoms in the outer of interfacial zone precipitate as δ-Mg. Meanwhile, Al and Zn atoms precipitate as α(Al)(Zn) in the inner of the interfacial zone. Almost all Al atoms are bonded with Zn atoms. Ti atoms in the TC4 substrate have

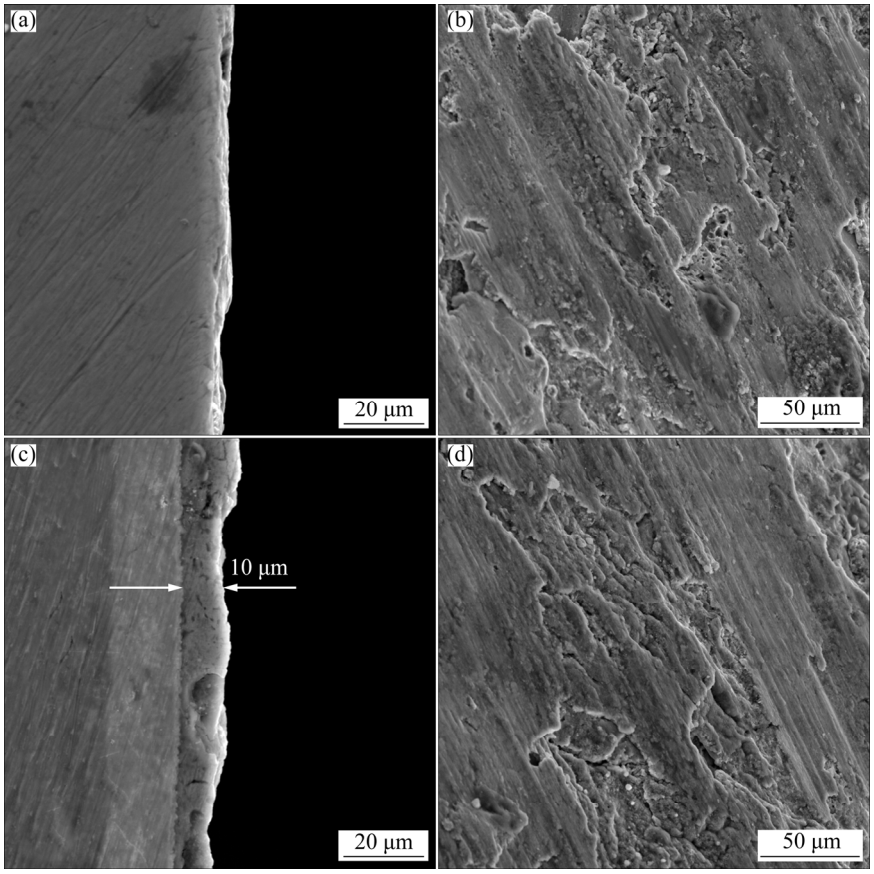

Fig. 15 Typical fracture surfaces of TC4/AZ91D bimetallic materials cast at 720 °C: (a, b) Al interlayer; (c, d) Zn/Al composite interlayer

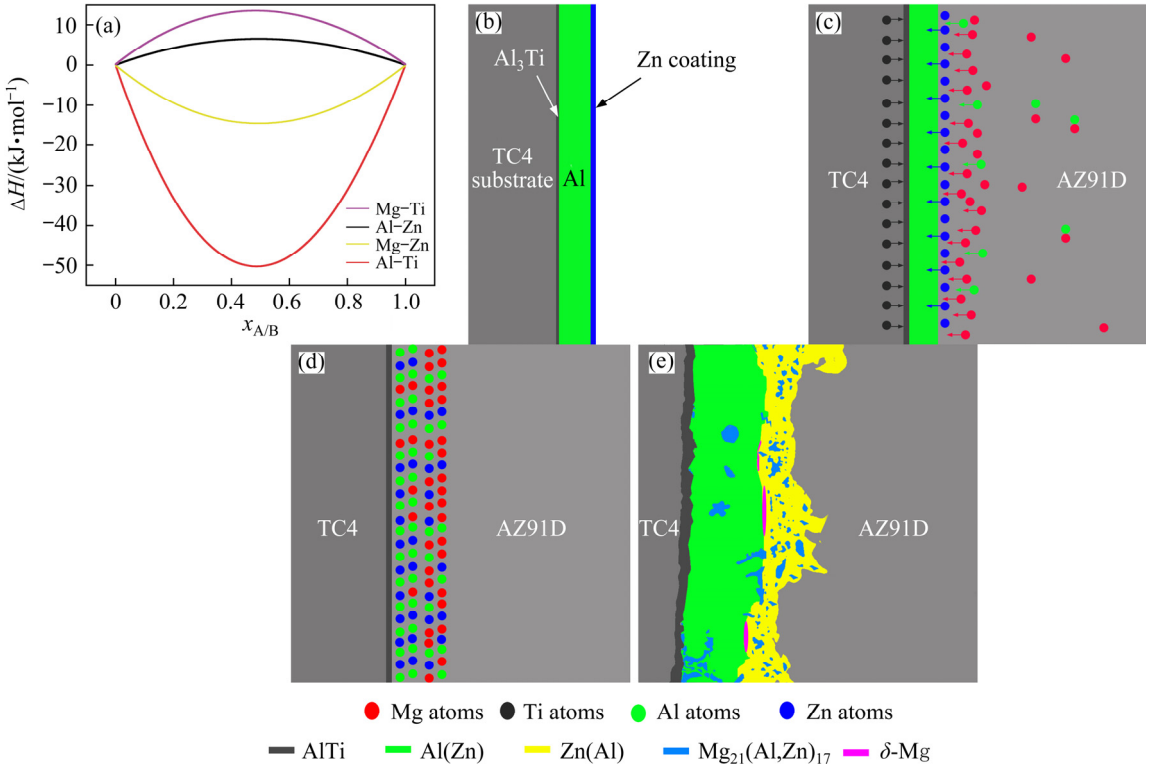

Fig. 16 Schematic diagrams showing bonding mechanism of TC4/AZ91D bimetal with Zn/Al composite interlayer: (a) Formation enthalpy change of binary system; (b) Before casting; (c) Filling process; (d) Enrichment of different kinds of atoms; (e) TC4/AZ91D bimetal after solidification

to react with $TiAl_3$ intermetallic compound and form AlTi by a spontaneous reaction [22,23]:

$$2Ti+TiAl_3 \rightarrow 3AlTi \quad (13)$$

Due to different reaction sequences and reaction products, different diffusion reaction layers will be formed across the interface, and the whole interface of solid−liquid compound casting is formed finally.

4 Conclusions

(1) Zn/Al-coated TC4/AZ91D bimetal was produced successfully by SLCC method. The shear strength of TC4/AZ91D bimetal with Zn/Al composite interlayer is much higher than that with pure Al interlayer, and the shear strength is increased from 48.5 to 67.4 MPa.

(2) The main phases across the interfacial zone of Al-coated TC4/AZ91D bimetal are: $Al_{12}Mg_{17}$ + δ-Mg eutectic structure and AlMgTi ternary structure. With the application of Zn/Al composite interlayer, α(Al)(Zn) + $Mg_{21}(Al,Zn)_{17}$ takes place of $Al_{12}Mg_{17}$ + δ-Mg eutectic structure in the interfacial zone, which prevents the formation of $Al_{12}Mg_{17}$ phase.

(3) The reason that the solid solution structure replaces $Al_{12}Mg_{17}$ + δ-Mg eutectic structure can be explained based on the thermodynamic analysis in details, which provides the theoretical basis for the main conclusions of this work.

Acknowledgments

The authors are grateful for the financial support from the National Natural Science Foundation of China (No. 51875062).

References

[1] LU Xing, ZHAO Guo-qun, XI Hua-kun, ZHANG Cun-sheng, CHEN Liang, SUN Lu. Microstructure, mechanical properties and welding quality evaluation of longitudinal welds in hollow magnesium alloy profiles extruded at different ram speeds [J]. Materials Characterization, 2019, 151: 414−428.

[2] NIE Hui-hui, ZHENG Liu-wei, KANG Xiao-ping, HAO Xin-wei, LI Xian-rong, LIANG Wei. In-situ investigation of deformation behavior and fracture forms of Ti/Al/Mg/Al/Ti laminates [J]. Transactions of Nonferrous Metals Society of China, 2021, 31(6): 1656−1664.

[3] DENG Yun-hua, GUAN Qiao, TAO Jun. Effect of heating time on bonding interface, atom diffusion and mechanical properties of dissimilar titanium joints produced by thermal self-compressing bonding [J]. Transactions of Nonferrous Metals Society of China, 2018, 28(4): 662−668.

[4] FENG Guang-jie, WEI Yan, HU Bing-xu, WANG Yi-feng, DENG De-an, YANG Xiu-xia. Vacuum diffusion bonding of Ti_2AlNb alloy and TC4 alloy [J]. Transactions of Nonferrous Metals Society of China, 2021, 31(9): 2677−2686.

[5] REN Li-rong, QIN Shui-jie, ZHAO Si-hao, XIAO Hua-qiang. Fabrication and mechanical properties of Ti_2AlC/TiAl composites with co-continuous network structure [J]. Transactions of Nonferrous Metals Society of China, 2021, 31(7): 2005−2012.

[6] AONUMA M, NAKATA K. Effect of alloying elements on interface microstructure of Mg–Al–Zn magnesium alloys and titanium joint by friction stir welding [J]. Materials Science and Engineering B, 2009, 161(1−3): 46−49.

[7] LI Rui-di, LI Jing-long, XIONG Jiang-tao, ZHANG Fu-sheng, ZHAO Ke, JI Cheng-zhong. Friction heat production and atom diffusion behaviors during Mg−Ti rotating friction welding process [J]. Transactions of Nonferrous Metals Society of China, 2012, 22(11): 2665−2671.

[8] SAMAVATIAN M, KHODABANDEH A, HALVAEE A, AMADEH A A. Transient liquid phase bonding of Al 2024 to Ti−6Al−4V alloy using Cu−Zn interlayer [J]. Transactions of Nonferrous Metals Society of China, 2015, 25(3): 770−775.

[9] CAO R, FENG Z, CHEN J H. Microstructures and properties of titanium–copper lap welded joints by cold metal transfer technology [J]. Materials & Design, 2014, 53: 192−201.

[10] XU Chuan, SHENG Guang-min, WANG Hui, FENG Ke, YUAN Xin-jian. Tungsten inert gas welding-brazing of AZ31B magnesium alloy to TC4 titanium alloy [J]. Journal of Materials Science & Technology, 2016, 32(2): 167−171.

[11] GAO Ming, MEI Shu-wen, LI Xiang-you, ZENG Xiao-yan. Characterization and formation mechanism of laser-welded Mg and Al alloys using Ti interlayer [J]. Scripta Materialia, 2012, 67(2): 193−196.

[12] TAN Cai-wang, CHEN Bo, MENG Sheng-hao, ZHANG Kai-ping, SONG Xiao-guo, ZHOU Li, FENG Ji-cai. Microstructure and mechanical properties of laser welded-brazed Mg/Ti joints with AZ91 Mg based filler [J]. Materials & Design, 2016, 99: 127−134.

[13] TAN Cai-wang, SONG Xiao-guo, CHEN Bo, LI Li-qun, FENG Ji-cai. Enhanced interfacial reaction and mechanical properties of laser welded-brazed Mg/Ti joints with Al element from filler [J]. Materials Letters, 2016, 167: 38−42.

[14] JIANG Zai-liang, FAN Zi-tian, JIANG Wen-ming, LI Guang-yu, WU Yao, GUAN Feng, JIANG Hai-xiao. Interfacial microstructures and mechanical properties of Mg/Al bimetal produced by a novel liquid−liquid compound casting process [J]. Journal of Materials Processing Technology, 2018, 261: 149−158.

[15] ZHAO Jian-hua, ZHAO Wen-qun, QU Shen, ZHANG Yan-qing. Microstructures and mechanical properties of AZ91D/0Cr19Ni9 bimetal composite prepared by liquid−solid compound casting [J]. Transactions of Nonferrous Metals Society of China, 2019, 29(1): 51−58.

[16] CHEN Dan, JIANG Yi-hui, LI Yu-fa, LIU Di, HE Jiang-tan,

CAO Fei, LIANG Shu-hua. In situ TiB_2/Cu composites fabricated by spray deposition using solid−liquid and liquid−liquid reactions [J]. Transactions of Nonferrous Metals Society of China, 2020, 30(7): 1849−1856.

[17] MURRAY J L. The Mg−Ti (magnesium−titanium) system [J]. Bulletin of Alloy Phase Diagrams, 1986, 7(3): 245−248.

[18] WEN Fu-lin, ZHAO Jian-hua, YUAN Miao-wang, WANG Jing-feng, ZHENG Deng-zhi, ZHANG Jin-yong, HE Ke, SHANGGUAN Jing-jing, GUO Yu. Influence of Ni interlayer on interfacial microstructure and mechanical properties of Ti−6Al−4V/AZ91D bimetals fabricated by a solid–liquid compound casting process [J]. Journal of Magnesium and Alloys, 2021, 9(4): 1382−1395.

[19] CHEN M R, JIANG Y, HE Y H, LIN L W, HUANG B Y, LIU C T. Pore evolution regulation in synthesis of open pore structured Ti−Al intermetallic compounds by solid diffusion [J]. Journal of Alloys and Compounds, 2012, 521: 12−15.

[20] JAFARI R, EGHBALI B, ADHAMI M. Influence of annealing on the microstructure and mechanical properties of Ti/Al and Ti/Al/Nb laminated composites [J]. Materials Chemistry and Physics, 2018, 213: 313−323.

[21] JENG S C. Oxidation behavior and microstructural evolution of hot-dipped aluminum coating on Ti−6Al−4V alloy at 800 °C [J]. Surface and Coatings Technology, 2013, 235: 867−874.

[22] HU Yuan-tao, ZHENG Lei, YAN Hao-jie, WU Lian-kui, LIN Xiang-jun, CAO Fa-he, JIANG Mei-yan. Improving hot corrosion resistance of aluminized TiAl alloy by anodization and pre-oxidation [J]. Transactions of Nonferrous Metals Society of China, 2021, 31(1): 193−206.

[23] JIANG Shu-ying, LI Shi-chun, ZHANG Lei. Microstructure evolution of Al−Ti liquid–solid interface [J]. Transactions of Nonferrous Metals Society of China, 2013, 23(12): 3545−3552.

[24] NASSIK M, CHRIFI-ALAOUI F Z, MAHDOUK K, GACHON J C. Calorimetric study of the aluminium–titanium system [J]. Journal of Alloys and Compounds, 2003, 350: 151−154.

[25] MIEDEMA A R. Energy effects and charge transfer in metal physics; modelling in real space [J]. Physica B: Condensed Matter, 1992, 182: 1−17.

[26] MIRIYEV A, LEVY A, KALABUKHOV S, FRAGE N. Interface evolution and shear strength of Al/Ti bi-metals processed by a spark plasma sintering (SPS) apparatus [J]. Journal of Alloys and Compounds, 2016, 678: 329−336.

[27] FANG C M, FAN Z. An ab initio study on stacking and stability of $TiAl_3$ phases [J]. Computational Materials Science, 2018, 153: 309−314.

[28] HU Hai, WU Xiao-zhi, WANG Rui, JIA Zhi-hong, LI Wei-guo, LIU Qing. Structural stability, mechanical properties and stacking fault energies of $TiAl_3$ alloyed with Zn, Cu, Ag: First-principles study [J]. Journal of Alloys and Compounds, 2016, 666: 185−196.

[29] LI Rui-qing. The application of *R* function to new asymmetric model and Toop model [J]. Calphad, 1989, 13(1): 67−70.

[30] KEŞLIOĞLU K, MARAŞLI N. Solid–liquid interfacial energy of the eutectoid β phase in the Al−Zn eutectic system [J]. Materials Science and Engineering A, 2004, 369(1/2): 294−301.

Zn/Al 中间层液固复合铸造制备 TC4/AZ91D 双金属复合材料的显微组织和力学性能

赵建华[1,2]，上官晶晶[1]，辜 诚[1]，靳炳岩[1]，石 禹[1]

1. 重庆大学 材料科学与工程学院，重庆 400044；
2. 重庆大学 机械传动国家重点实验室，重庆 400044

摘 要：为了获得高强度、具有冶金结合界面的 Ti/Mg 双金属复合材料，通过热浸镀铝方法在 TC4 钛合金表面制备 Al 涂层并在热浸镀铝 TC4 表面进一步采用电镀锌工艺制备 Zn/Al 复合层。采用液固复合铸造方法制备具有冶金结合界面的 TC4/AZ91D 双金属复合材料。结果表明：当采用 Zn/Al 复合中间层时，界面组成为 AlTi 和 α(Al) + $Mg_{21}(Al,Zn)_{17}$；而仅采用 Al 中间层时，界面组成主要为 AlMgTi 三元组织和 $Al_{12}Mg_{17}$ + δ-Mg 共晶组织。相比 Al 中间层，采用 Zn/Al 复合中间层的 TC4/AZ91D 的剪切强度从 48.5 MPa 提高到 67.4 MPa。此外，根据界面的不同组成成分建立热力学模型有助于解释界面区域的组织演变过程。

关键词：Ti/Mg 双金属复合材料；液固复合铸造；热力学分析；显微组织；力学性能

(Edited by Wei-ping CHEN)